



Felicetti, L., Harkness, P., and Ceriotti, M. (2017) Attitude and Orbital Dynamics of a Variable-Geometry, Spinning Solar Sail in Earth Orbit. In: Fourth International Symposium on Solar Sailing (ISSS 2017), Kyoto, Japan, 17-20 Jan 2017.

This is the author's final accepted version.

There may be differences between this version and the published version. You are advised to consult the publisher's version if you wish to cite from it.

<http://eprints.gla.ac.uk/135224/>

Deposited on: 24 January 2017

Attitude and Orbital Dynamics of a Variable-Geometry, Spinning Solar Sail in Earth Orbit

By Leonard FELICETTI¹⁾²⁾, Patrick HARKNESS²⁾ and Matteo CERIOTTI²⁾

¹⁾Luleå University of Technology, Kiruna, Sweden

²⁾University of Glasgow, Glasgow, United Kingdom

(Received 1st Dec, 2016)

At the ISSS 2013, a novel concept of variable-geometry solar sail was introduced: deployed in the shape of a three-dimensional quasi-rhombic pyramid (QRP), the sail exploited its shape and shift between center of mass and center of pressure to naturally achieve heliostability (stable sun-pointing) throughout the mission. In addition, mechanisms allowed to vary the flare angle of the four booms in opposite pairs, thus allowing to control the area exposed to the sun without the need of slew maneuvers. Using these adjustments in favorable orbital positions, it is possible to build a regular pattern of acceleration to achieve orbit raising or lowering without the need of propulsion system or attitude control. Subsequent more detailed investigations revealed that eclipses, even if lasting only a fraction of the orbit, have a substantial (and negative) impact on the heliostability effect: and even a small residual angular velocity, or disturbance torque, are enough to cause the spacecraft to tumble. In this work, we present a novel and improved concept which allows the sail to preserve its attitude not only with eclipses, but also in presence of disturbance torques such as the gravity gradient. The solution we propose is to add a moderate spin to the solar sail, combined with ring dampers. The gyroscopic stiffness due to the spin guarantees stability during the transient periods of the eclipses, while the heliostability effect, combined with the dampers, cancels any residual unwanted oscillation during the parts of the orbit exposed to the sun, and at the same time guarantees continuous sun-pointing as the apparent direction of the sun rotates throughout the year. Both theoretical and numerical analyses are performed. First, stability bounds on the sail design are calculated, obtaining conditions on the flare angles of the sail, in the different orbital regimes, to test the robustness of the concept. Then, a numerical analysis is performed to validate the study in a simulated scenario where all perturbations are considered, over extended amount of time. The concept targets equatorial orbits above approximately 5,000 km. Results show that an increase of 2,200 km per year for a small device at GEO can be achieved with a CubeSat-sized sail.

Nomenclature

$\mathbf{1}$	= Identity matrix	P_s	= Solar radiation pressure at Earth distance, $4.56 \times 10^{-6} \text{ N/m}^2$
a_1, a_2, a_4	= Coefficients of the characteristic equation	\mathbf{q}	= $[\alpha_1, \alpha_2]^T$
\mathbf{a}	= Acceleration vector, m/s^2	\mathbf{r}	= Position vector, m or km
b	= Quasi-rhombic pyramid base length, m	r	= Distance from the Earth's center, km
$\hat{\mathbf{c}}_1, \hat{\mathbf{c}}_2, \hat{\mathbf{c}}_3$	= Axes of the inertial reference frame	R_E	= Radius of the Earth, 6371 km
c_f	= Rotational damping coefficient, N m/rad s	$\hat{\mathbf{r}}_s$	= Sun direction
d	= Distance to principal axis of inertia, m	\mathbf{v}	= Velocity vector, km/s
f	= True anomaly, rad	t	= Time, hours or days
$f_{control}$	= Angle for orbital control law, rad	\mathbf{T}	= Torque vector, N m
\mathbf{F}	= Force, N	$\hat{\mathbf{t}}$	= Unit vector tangent to plane
\mathbf{G}	= Gyro Matrix	S	= Surface of each sail face, m^2
\mathbf{h}	= Orbital angular momentum vector per unit mass, km^2/s	z_{CM}	= Offset between the center of mass and the center of pressure of the sail, m
h	= Module of the orbital angular momentum per unit mass, km^2/s	$\hat{\mathbf{x}}, \hat{\mathbf{y}}, \hat{\mathbf{z}}$	= Body axes
i	= Inclination, deg	α	= Apex angle of the sail's surfaces, deg
I	= Moment of inertia, kg m^2	$\boldsymbol{\alpha}$	= Vector of small angular deviation from the pure spin motion, rad
\mathbf{I}	= Inertia matrix, kg m^2	$\alpha_1, \alpha_2, \alpha_3$	= Small angular deviations from the pure spin motion w.r.t. body axes, rad
k_1, k_2	= Pitch and yaw inertia ratios	β	= Precession cone angle, deg
\mathbf{K}	= Stiffness matrix	γ	= Pointing angle, deg
l	= Length of booms, m	$\boldsymbol{\Gamma}$	= Sail angular momentum, $\text{kg m}^2/\text{s}$
m	= Mass, kg	Δ	= Nutation angle, deg
\mathbf{M}	= Mass matrix	ε	= Obliquity of equator on the ecliptic, 23.5°
$\hat{\mathbf{n}}$	= Unit vector normal to plane	η	= Sail efficiency
n_0	= Mean motion, rad/s	θ	= Boom flare angle, deg

λ	=	Longitude of the Sun, deg
μ	=	Planetary constant of the Earth, 3.986×10^5 km^3/s^2
ω_0	=	Nominal spin rate, rad/s
$\boldsymbol{\omega}$	=	Angular velocity vector in body axes, rad/s
$\boldsymbol{\omega}_0$	=	Nominal angular velocity vector in body axes, rad/s

Superscripts

<i>closed</i>	=	sail in fully closed configuration
<i>damp</i>	=	damping
<i>eclipse</i>	=	sail in eclipse mode configuration
<i>open</i>	=	sail in fully open configuration
<i>(ECI)</i>	=	Earth-centered inertial frame

Subscripts

0	=	At initial time
A, B	=	Boom A, B
CM	=	Center of mass
d	=	Disturbance
gg	=	Gravity gradient
h	=	Along the out-of-plane direction
i	=	i -th face
<i>membrane</i>	=	Sail membrane
n	=	Along the normal direction
O	=	Origin of the body reference frame
s	=	Sun
t	=	Along the tangential direction
<i>sail</i>	=	Sail
x, y, z	=	Components w.r.t. body axes

Operators

c_{\square}	=	$\cos(\square)$
s_{\square}	=	$\sin(\square)$
$[\square \times]$	=	Skew-symmetric matrix

1. Introduction

During the 3rd International Symposium on Solar Sailing 2013 in Glasgow, UK, Ceriotti et al.¹⁾ presented a novel configuration for a variable-geometry solar sail spacecraft. Named the quasi-rhombic pyramid (QRP), it consists of spacecraft bus which deploys booms along the slant edges, such that reflective membranes may fill the slant faces, and the bus itself remains at the apex of the pyramid. The center of solar pressure is therefore more distant from the apex than the center of mass (a distance we term the heliostatic margin), and the spacecraft accordingly exhibits longitudinal heliostatic stability. If undamped, the motion in response to a disturbance is a quasi-harmonic oscillation about the equilibrium position.

The rationale behind this new concept was that solar sails require some form of control over the direction and magnitude of the thrust produced by the solar sail has usually been required²⁾. It has been suggested that the solar sail can be tilted, using moving masses or propellant, as part of an active attitude and orbit control system³⁾ and that the thrust vector can be modified by changing the reflectivity of the membrane⁴⁾.

However the required attitude control becomes challenging in Earth orbit, where the short orbital periods require rapid slew

maneuvers of the sail, and indeed some conventional actuators⁵⁾ will likely struggle due to the high moments of inertia associated with typical deployed sails. This issue becomes critical in the nanosatellite regime, where the constraints in power and size significantly affect the capabilities of the attitude control system, and even solutions involving changes to the reflectivity of the sail are unlikely to be successful⁴⁾. That work described several research contributions to solar sailing in Earth orbit using mostly traditional, square sails, showing the QRP approach offers some distinct advantages. For example, the shape-changing maneuver can be conducted without the need for momentum wheels to execute two slews per orbit, and there are no out-of-plane forces generated during the transition itself. More generally, the overall magnitude of the SRP force generated by the sail can be ‘throttled’ by adjusting the flare angle without any undesired force components being generated at all, which is something only previously achievable using techniques based on changing the reflectivity of the membrane⁶⁾.

Ceriotti et al.¹⁾ showed that a QRP-sail can be used to raise or decrease the altitude of a small satellite in a range of circular, equatorial orbits (although this concept is not limited to these). This is achieved by opening the sail such that the solar radiation pressure (SRP) provides an accelerating force as the satellite moves away from the Sun, and then closing it to minimize the braking force in the second half of the orbit. By operating a QRP-sail in this manner, it was shown that the orbit can be raised significantly, especially at higher altitudes (e.g. GEO) where grave-yarding at end-of-life is particularly important. In addition, the control law can easily be reversed to achieve an orbit lowering effect if desired, for example to initiate an orbital transfer that would eventually lead to atmospheric re-entry.

The concept is obviously limited by atmospheric drag, but above the upper atmosphere both orbit raising and orbit lowering may be achieved by harnessing the action of sunlight alone.

In addition, Ceriotti et al.¹⁾ assumed that the heliostabilising effect of the sun was constantly present. This is, however, not true in low-inclination Earth orbits, where eclipses may occupy a large fraction of the orbit, depending on the altitude. During the eclipse phase, the solar radiation pressure is essentially null, and any residual angular velocity of the spacecraft will not be counteracted by the heliostability effect. It can be shown that this can initiate larger oscillations, eventually leading to uncontrolled tumbling.

In this paper, we propose to extend the previous work to include the effects of the eclipses. We achieve so by adding a spin along the pyramid axis. During the eclipse phase, additional stability is provided by the axial spin, which maintains the nominal attitude during eclipse, and we note that disturbances are minimized because operation of the QRP requires (and results) in no net torque being applied about the spacecraft itself. The satellite could be released in a spinning state, or the spin could be initiated, for example, through the heliogyro effect or cold jet thrusters.

The paper is organized as follows: Section 2 is devoted to describing the QRP sail concept, providing the reference frames, the model for the solar radiation acting upon the sail surfaces, the attitude and orbital dynamics, and the orbit control

law. Section 3 addresses the attitude stabilization analytically by applying linearized models and then using the Routh-Hurwitz criterion to obtain useful bounds for the sail design. Finally the numerical results, provided in Section 4, illustrate the expected performance of the sail as well as the robustness of the control strategies against perturbations arising from eclipse, gravity gradient, and the Sun's motion on the ecliptic.

2. The Quasi Rhombic Pyramid Concept

2.1. Geometry, mass and forces

The QRP spacecraft is composed of a central bus at the apex of a pyramidal sail as depicted in Fig. 1. This paper considers that the booms and membranes have already been deployed, that the structure is rigid, and that any transients have been damped.

The size and the shape of each triangular face of the QRP cannot be altered if the membrane is to remain taut, so the four triangular faces are modelled as very thin rigid bodies connected to the booms. The length of base of a triangle is b and the length of the booms is l . Two different sail configurations, as the booms move in opposing pairs (θ_A for one pair, θ_B for the opposite pair), are also shown in Fig. 1.

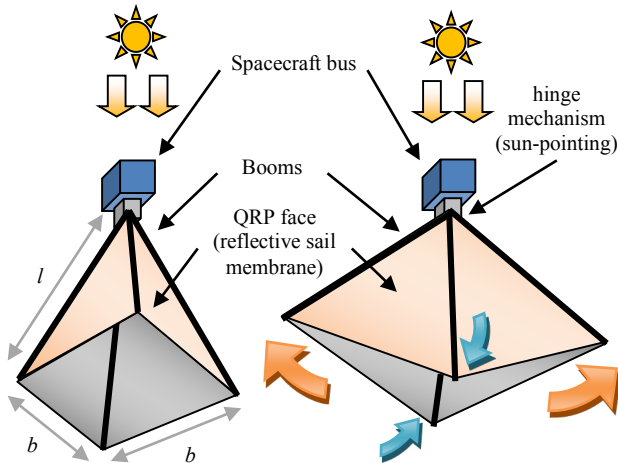


Fig. 1. The quasi-rhombic pyramid concept (QRP).

A uniform areal density σ of the sail material is calculated, taking into account the mass of the booms, while the overall mass of the spacecraft m has two contributions: one due to the sail assembly and one due to the spacecraft bus, which is a uniform cube of side l_{bus} . The centroids of faces of the sail are the points where the solar radiation force, as calculated by integrating the SRP along the surface, is applied. For details on the geometry of the spacecraft and its inertia, we refer the reader to Ceriotti et al.⁷⁾. The net force generated by the SRP on each partially reflecting face i , due to specular reflection and absorption, is⁸⁾:

$$\mathbf{F}_i = -(1+\eta)P_s S(\hat{\mathbf{n}}_i \cdot \hat{\mathbf{r}}_s)^2 \hat{\mathbf{n}}_i - (1-\eta)P_s S(\hat{\mathbf{n}}_i \cdot \hat{\mathbf{r}}_s)(\hat{\mathbf{t}}_i \cdot \hat{\mathbf{r}}_s)\hat{\mathbf{t}}_i \quad (1.)$$

where $P_s = 4.56 \times 10^{-6} \text{ N/m}^2$ is the SRP at 1 Astronomical Unit from the Sun, S is the face area, $\hat{\mathbf{n}}_i$ and $\hat{\mathbf{t}}_i$ are the normal and tangential direction respectively, which can be expressed

as in Hughes⁹⁾, pp. 253. Each face is assumed to have perfectly specular reflectivity and no thermal reemission, but will still have an overall reflectivity efficiency η less than unity due to absorption (note Ceriotti et al.¹⁾ did not consider absorption). The main effect of absorption is to reduce the acceleration magnitude and to introduce a force component tangential to the surface¹⁰⁾ as pointed by $\hat{\mathbf{t}}_i$.

In Eq. (1.), the direction $\hat{\mathbf{r}}_s$ can easily be calculated, in an Earth Centered Inertial reference frame (ECI) as function of time, by means of¹¹⁾ $\hat{\mathbf{r}}_s^{(ECI)} = [\cos \lambda \quad \sin \lambda \cos \varepsilon \quad \sin \lambda \sin \varepsilon]^T$, $\lambda = \lambda_0 + t\dot{\lambda}$, where λ is the longitude of the Sun, $\dot{\lambda} = 1.99 \cdot 10^{-7} \text{ rad/s}$ is the angular velocity of the Earth-Sun system (assumed constant), and $\varepsilon = 23.5 \text{ deg}$ is the obliquity of the equator on the ecliptic plane. By choosing $\lambda_0 = 0$, then at time $t=0$ the Sun is at the vernal equinox in the equatorial plane.

The force \mathbf{F}_i is only experienced on a face lit by the Sun, i.e. $\hat{\mathbf{n}}_i \cdot \hat{\mathbf{r}}_s > 0$. As it is considered that the sun is always on the apex side of the device partial illumination of faces does not occur and the total acceleration experienced by the sail \mathbf{a}_{sail} is simply the sum of the contributions of all the four faces. Torque about the center of mass \mathbf{T}_{sail} may similarly be calculated.

2.2. Attitude dynamics

The attitude of the QRP sail is described with a rigid body model and the changes in boom configuration are assumed to be instantaneous. The equation of motion for the angular velocity of the sail can be written as¹²⁾:

$$\mathbf{I}\dot{\boldsymbol{\omega}} = -\boldsymbol{\omega} \times \mathbf{I}\boldsymbol{\omega} + \mathbf{T}_{sail} + \mathbf{T}_d \quad (2.)$$

The SRP torque \mathbf{T}_{sail} is computed with the correct value of the inertial matrix \mathbf{I} being used according to the flare angle of the booms and the current configuration of the sail. \mathbf{T}_d contains any disturbance torques such as nutation damping and gravity gradient, which is itself modelled as (Schaub et al.¹²⁾, pp.188-191):

$$\mathbf{T}_{d,gg} = \frac{3\mu}{r^5} \mathbf{r} \times \mathbf{I} \mathbf{r} \quad (3.)$$

where μ is the planetary constant ($\mu = 3.986 \times 10^5 \text{ km}^3/\text{s}^2$). Attitude parameterization is performed by using quaternions (Schaub et al.¹²⁾, pp.103-104) to obtain the direction of the Sun $\hat{\mathbf{r}}_s$ in body axes, as required in Eq. (1.). Expressions of the damping torque will be provided in Section 3.

2.3. Orbital dynamics

For the purposes of orbital propagation, the Earth's gravity, secular effects due to the Earth's oblateness, and the effect of SRP are considered. Aerodynamic effects are neglected because the lowest orbits in this study are above 1000 km.

The differential equation of motion of the spacecraft, neglecting the Earth's oblateness for the moment, is:

$$\ddot{\mathbf{r}}^{(ECI)} = -\frac{\mu}{r^2} \hat{\mathbf{r}}^{(ECI)} + \mathbf{a}_{sail}^{(ECI)} \quad (4.)$$

where \mathbf{r} is the position vector and $\mathbf{a}_{sail}^{(ECI)}$ the acceleration due to the solar radiation both expressed in ECI reference frame.

Due to the magnitude of the perturbing accelerations with respect to the gravitational acceleration, all the Keplerian elements of the orbit except from the true anomaly, f , change very slowly and so the integration is performed using Gauss' variational equations (Battin¹³), pp. 488-489). The secular effect due to Earth's oblateness, or J_2 , is then considered, in terms of regression of the nodes and advance of perigee, where the secular rates can be described as function of semimajor axis, inclination and eccentricity of the orbit (Schaub et al.¹²), pp. 581-583). Finally, eclipses are modelled without a penumbra, and the spacecraft is considered to be in eclipse when it is inside the ideal cylinder of shadow cast by the Earth. When the spacecraft is in an eclipse condition, $\mathbf{F}_i = 0$, no SRP force and torque are experienced, and therefore the equations of motion are integrated with $\mathbf{a}_{sail} = 0$ and $\mathbf{T}_{sail} = 0$.

2.4. Control Law

This mission concept is intended to allow either an increase or a decrease in the semi-major axis by opening or closing the sail booms in order to control the thrust provided by the SRP. Ceriotti et al.¹⁾ showed that, to increase the semi-major axis, the sail (in its nominal sun-pointing attitude) should be open when the spacecraft is travelling away from the Sun, and it should be as closed as possible when the spacecraft is travelling towards the Sun. This is equivalent to the following condition for open sail (see Fig. 2):

$$\text{acos}(-\hat{\mathbf{r}}_s \cdot \hat{\mathbf{v}}) < f_{control} \quad (5.)$$

where the angle $f_{control} \in [0, \pi/2]$ is a control law parameter and can be arbitrarily selected by taking into account some constraints like the eclipse conditions.

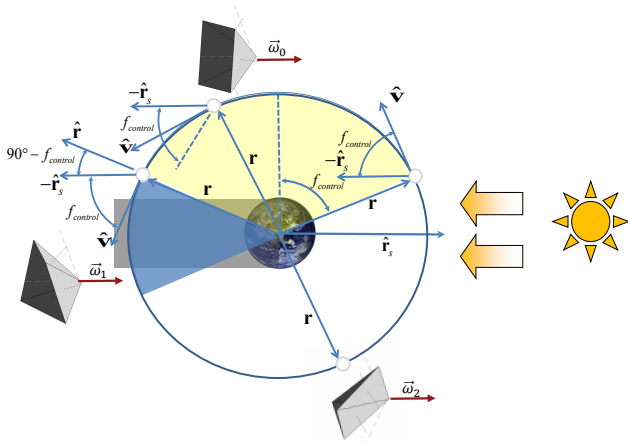


Fig. 2. Orbit control and phases during the orbit.

However, Fig. 2 shows that there is one more phase to take into account: the eclipse. In this region heliostability effects are lost and small perturbations such as gravity gradient, or even residual angular velocities, can build up to large attitude deviations from the sun-pointing direction unless the sail is reconfigured in order to reduce the unwanted drift. The change of the sail configuration should be performed before the

spacecraft enters into the eclipse in order to exploit the remaining heliostability to settle the sail after the shape-changing maneuver, as soon as the following condition is satisfied:

$$\arccos(-\hat{\mathbf{r}}_s \cdot \hat{\mathbf{r}}) < \frac{\pi}{2} - f_{control} \quad (6.)$$

In conclusion, an additional phase is added to the orbit, leading to three different sail configurations:

- Sail fully open, when the spacecraft is travelling away from the sun, to maximize the increase in semimajor axis;
- Sail partially open, during the eclipse phase, to minimize the impact of perturbations on the attitude, in absence of SRP;
- Sail fully closed, when the spacecraft is travelling towards the sun, to minimize the acceleration, which would mainly be against the velocity vector.

3. Attitude Stabilization and Control

The spacecraft nominal attitude is sun-pointing, and to counteract losses of stability associated with the eclipses, the spacecraft is spun around the $\hat{\mathbf{z}}$ body axis. The attitude stability properties in both the illuminated and eclipse phases can be analyzed by linearizing the equations around the nominal configuration of the sail, and considering small displacements of the spin axis with respect to the sun direction, as represented in Fig. 3.

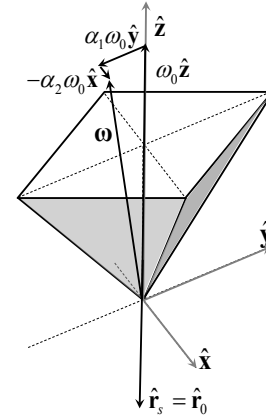


Fig. 3. Small angular deviation with respect to the nominal spin motion.

Specifically, let us suppose that the spacecraft is spinning around its principal axis $\hat{\mathbf{z}}$ with a nominal angular velocity $\boldsymbol{\omega}_0 = \omega_0 \hat{\mathbf{z}}$. Let us also consider small angular deviations from the pure spin motion $\boldsymbol{\alpha} = [\alpha_1 \ \alpha_2 \ \alpha_3]$ with respect to the three body axes respectively, and the corresponding small changes in angular velocity $\dot{\boldsymbol{\alpha}} = [\dot{\alpha}_1 \ \dot{\alpha}_2 \ \dot{\alpha}_3]$. The resulting angular velocity can be expressed as follows:

$$\boldsymbol{\omega} = (\mathbf{1} - [\boldsymbol{\alpha} \times]) \boldsymbol{\omega}_0 + \dot{\boldsymbol{\alpha}} = \begin{bmatrix} -\alpha_2 \omega_0 + \dot{\alpha}_1 \\ \alpha_1 \omega_0 + \dot{\alpha}_2 \\ \omega_0 + \dot{\alpha}_3 \end{bmatrix} \quad (7.)$$

where $\mathbf{1}$ is the identity matrix and $[\boldsymbol{\alpha} \times]$ is the skew-symmetric matrix obtained with components of $\boldsymbol{\alpha}$. By substituting Eq. (7.) into Eq. (2.) and by neglecting the higher-order terms, one can obtain the following linearized equation of motion about the

nominal spin motion for yaw and pitch in matrix form (roll is completely decoupled) (Hughes⁹, pp. 116-121):

$$\mathbf{M}\dot{\mathbf{q}} + \mathbf{G}\dot{\mathbf{q}} + \mathbf{K}\mathbf{q} = \mathbf{T} \quad (8.)$$

where:

$$\mathbf{M} = \begin{bmatrix} I_x & 0 \\ 0 & I_y \end{bmatrix}; \mathbf{q} = \begin{bmatrix} \alpha_1 \\ \alpha_2 \end{bmatrix}; \mathbf{G} = \omega_0 (I_x + I_y - I_z) \begin{bmatrix} 0 & -1 \\ +1 & 0 \end{bmatrix}$$

$$\mathbf{K} = \omega_0^2 \begin{bmatrix} (I_z - I_y) & 0 \\ 0 & (I_z - I_x) \end{bmatrix}; \mathbf{T} = \begin{bmatrix} T_x \\ T_y \end{bmatrix}$$

The stability properties of the system are strictly connected to the characteristic equation of this system. In the following subsections three different stability conditions will be developed and analyzed for the three working conditions of the sail: the torque-free case, the illuminated case, and the eclipse case. In order to analyse the stability properties during these phases, some assumptions have been made and a candidate sail design point will be derived and discussed. To this end a parametric study will be performed, by considering a spacecraft with the fixed geometry and mass characteristics listed in Table 1, but varying the following parameters:

- length of the booms of the sail ($l = 1 \text{ m}$ and $l = 2 \text{ m}$)
- length of the base of the sail b ($0 \leq b \leq \sqrt{2}l$)
- flare angle θ_A ($0 \leq \theta_A \leq \alpha$)

where α is the apex angle of the sail surfaces.

The values in Table 1 are typical of a nanosatellite (CubeSat) and of technology used for the solar sails¹⁴). The nominal spin rate ω_0 is referred to a fully-open sail ($\theta_A = \theta_B$) and for the other configurations the angular velocity is computed as follows, using the conservation of angular momentum:

$$\boldsymbol{\omega}_1 = (\mathbf{I}_1)^{-1} (\mathbf{I}_0 \boldsymbol{\omega}_0) \quad (9.)$$

where the subscript 0 refers to the sail-open configuration and 1 to any different configuration. Thus, it is assumed that when the flare angle is changed the update is instantaneous and the angular velocity is modified with respect to Eq. (9).

Table 1. Spacecraft data.

Bus mass, m_{bus} , kg	1
Bus size, l_{bus} , cm	10
Boom linear density, ρ_{boom} , g/m	16.3
Sail membrane areal density, $\sigma_{membrane}$, g/m ²	13.2
Sail assembly mass per unit area, σ , kg/m ²	0.050
Sail reflectivity, η	0.85
Nominal spin rate, ω_0 , rph	10

3.1. Homogeneous (torque-free) motion

The stability of the system for an ideal torque-free case (free spinning rigid body) is studied first. The characteristic equation of the system reads as:

$$\det[\mathbf{M}s^2 + \mathbf{G}s + \mathbf{K}] = 0 \Rightarrow s^4 + a_1s^2 + a_2 = 0 \quad (10.)$$

where $a_1 = \omega_0^2(1 + k_1k_2)$, $a_2 = \omega_0^4k_1k_2$, $k_1 = (I_z - I_y)/I_x$ and $k_2 = (I_z - I_x)/I_y$. Therefore the application of the Routh-Hurwitz criterion leads to the well-known result that spin is stable around the largest or smallest axis of inertia of the

spacecraft (Hughes⁹, pp. 116-121), which can vary its alignment according to the instantaneous sail configuration.

Stable configurations ($k_1 > 0, k_2 > 0$) were identified as a function of the design ratio b/l of the sail and of the flare angle θ_A , for boom length $l = 1 \text{ m}$ and $l = 2 \text{ m}$ respectively.

It is noteworthy that different combinations b and θ_A produce both positive and negative values of the two inertia ratios and the stability conditions can be guaranteed only for a subset of the configuration space: small ranges of opening angles and high value of the lengths of the triangle base. The bottom-right halves of these plots, below the diagonal, have not been filled because they contain unfeasible configurations.

The stability analysis done so far does not take into account external torques but, during the three phases of the orbital motion the system is forced by the solar radiation torque and the gravity gradient torque. These do change the stability properties of the system as discussed below.

3.2. Illuminated phase

Due to the particular shape of the sail, the SRP provides a stabilizing torque which increases the stability region for the spin motion of the sail. The stability problem of the pitch-yaw motion of the sail can be analysed starting from Eq. (8.), where it is necessary to develop a linearized expression for the solar radiation torque. Equation (1.) can be rewritten as follows:

$$\mathbf{F}_i = -2\eta P_s S (\hat{\mathbf{n}}_i \cdot \hat{\mathbf{r}}_s)^2 \hat{\mathbf{n}}_i - (1 - \eta) P_s S (\hat{\mathbf{n}}_i \cdot \hat{\mathbf{r}}_s) \hat{\mathbf{r}}_s \quad (11.)$$

which can be used for calculating each contribution to the total solar torque due to each side of the sail as:

$$\mathbf{T}_{s,i} = (\mathbf{r}_{CM,i} - \mathbf{r}_{CM}) \times \mathbf{F}_i \quad (12.)$$

The full expression is omitted for conciseness. By assuming that the sail spin axis direction $\hat{\boldsymbol{\omega}}$ is nearly sun pointing, the attitude of the spacecraft can be represented again through a small angular displacement with respect to the nominal direction through $\boldsymbol{\alpha}$ as defined in Eq. (7.). In this case the direction of the nominal motion coincides with the sun direction $\hat{\mathbf{r}}_s$ and therefore, in the body reference frame, the direction $\hat{\mathbf{r}}_s$ can be expressed as:

$$\hat{\mathbf{r}}_s = [\mathbf{1} - [\boldsymbol{\alpha} \times]] \hat{\mathbf{r}}_{s,0} \quad (13.)$$

where $\hat{\mathbf{r}}_{s,0} = [0 \ 0 \ -1]^T$, as depicted in Fig. 3. Hence, adding up all the contributions of the sides of the sail in Eq. (12.), and by considering only the yaw-pitch motion, the total solar radiation torque can be rewritten in a matrix form as follows:

$$\mathbf{T}_{sail} = -[\mathbf{K}_{s,1} + \mathbf{K}_{s,2} + \mathbf{K}_{s,3} + \mathbf{K}_{s,4}] \begin{bmatrix} \alpha_1 \\ \alpha_2 \end{bmatrix} \quad (14.)$$

Where:

$$\mathbf{K}_{s,1} = \frac{16(1 + c_\alpha)\eta P_s S l}{3(1 - c_\alpha^2)^{3/2}} \begin{bmatrix} s_{\theta_A}^3 c_{\theta_B} s_{\theta_B} & 0 \\ 0 & s_{\theta_B}^3 c_{\theta_A} s_{\theta_A} \end{bmatrix}$$

$$\mathbf{K}_{s,2} = \frac{4(1 - \eta)P_s S l}{3\sqrt{1 - c_\alpha^2}} \begin{bmatrix} s_{\theta_A}(c_{\theta_A} s_{\theta_B} + 2s_{\theta_B} c_{\theta_B}) & 0 \\ 0 & s_{\theta_B}(c_{\theta_B} s_{\theta_A} + 2s_{\theta_A} c_{\theta_A}) \end{bmatrix}$$

$$\mathbf{K}_{s,3} = -16 \frac{\eta P_s S z_{CM}}{(1-c_\alpha^2)^{3/2}} \begin{bmatrix} s_{\theta_A}^3 s_{\theta_B} c_{\theta_B}^2 & 0 \\ 0 & s_{\theta_A} s_{\theta_B}^3 c_{\theta_B}^2 \end{bmatrix}$$

$$\mathbf{K}_{s,4} = -4 \frac{(1-\eta) P_s S z_{CM}}{\sqrt{1-c_\alpha^2}} \begin{bmatrix} s_{\theta_A} s_{\theta_B} & 0 \\ 0 & s_{\theta_A} s_{\theta_B} \end{bmatrix}$$

and $c_\alpha = 1 - b^2 / (2l^2)$.

It is noteworthy that Eq. (14.) shows linear relationship between torque and small angles α_1 and α_2 , but the coefficient matrix is dependent on the optical properties and on the shape of the sail. Specifically, these matrices are dependent on the two flare angles (θ_A, θ_B) which can be used as control variables. Furthermore, the offset between the center of mass and center of pressure of the sail – the heliostatic margin – also affects the system dynamics.

Inserting Eq. (14.) in Eq. (8.) leads to the following linearized system:

$$\mathbf{M}\ddot{\mathbf{q}} + \mathbf{G}\dot{\mathbf{q}} + [\mathbf{K} + \mathbf{K}_{s,1} + \mathbf{K}_{s,2} + \mathbf{K}_{s,3} + \mathbf{K}_{s,4}] \mathbf{q} = 0 \quad (15.)$$

Therefore, all the stability properties of the system may be modified by the SRP although we assume that the altitude is sufficient for SRP to dominate gravity gradient and aerodynamic effects. For now this simplifies the analysis by eliminating periodic coefficients but the parametric study, performed by decreasing the orbit altitude, will demonstrate the validity of the underlying hypothesis. Therefore, the new stability conditions can be found through the characteristic equation, applying again the Routh-Hurwitz criterion. These can be used to obtain the indicated flare angles during the illuminated phase, while the parametric study above indicates the configurations which are stable as the SRP is acts upon the sail. The analysis shows that two types of configurations lead to stability. Specifically, when the stiffness matrix given by the sum $\mathbf{K} + \mathbf{K}_{s,1} + \mathbf{K}_{s,2} + \mathbf{K}_{s,3} + \mathbf{K}_{s,4}$ is positive definite the system becomes statically stable, whereas the same matrix is negative definite the system is statically unstable but gyroscopically stabilized (Hughes⁹), pp.121-124). These results are shown in Fig. 4, where the two stable regions are shaded in different gray scales as a function of the base length and the flare angles for the nominal spin rate. These figures provide the upper and lower bounds of the flare angle for a given the pyramid base b ,

which should belong to the statically stable region. Once the sail has been designed (b has been assigned as shown in the dashed lines;), the only in-orbit control parameter for modifying the shape of the sail is the angle θ_A where the admissible range is determined by the intersection of the dashed line with the bounds of the stability region. Specifically, two working configurations can be chosen by means of these plots:

- the *fully-open* configuration maximizes the area exposed to the sun, in order to maximize the SRP thrust. This configuration is achieved when $\theta_A = \theta_B$ leading to¹⁾:

$$\cos \theta_{A,B} = \sqrt{\frac{2 - (b/l)^2}{2}} \quad (16.)$$

and, as a requirement for the sail design, this angle should be within the stable region.

- the *fully-closed* configuration minimizes the area exposed to the solar radiation. This configuration is defined by the lowest value of θ_A inside the stability region (along the ideal, horizontal line representing the selected length b).

3.3.Eclipse phase

When the spacecraft enters the eclipse, the stabilizing effect of the solar radiation torque disappear and the gravity gradient becomes the dominant forcing term. Therefore only the gyro-stiffness can counteract such perturbations and keep the sail pointing towards an inertially-fixed direction.

Some assumptions are made in order to analyse the stability in this phase. The equations of motion are linearized by assuming that both the sun direction and the spin axis coincide with the local vertical, which is reasonable as eclipse phases happen in the part of the orbit which is opposite to the sun with respect to the Earth. This work assumes that eclipses are short, or equivalently that the orbit is high, which is justified in two ways: a short eclipse means that the low-stability region lasts for a small fraction of the orbital period, while a high orbit means that the gravity gradient is dominated by SRP torque when not in eclipse. Numerical simulations in Section 4, taking into account the full attitude and orbital dynamics, will give quantitative results supporting this statement.

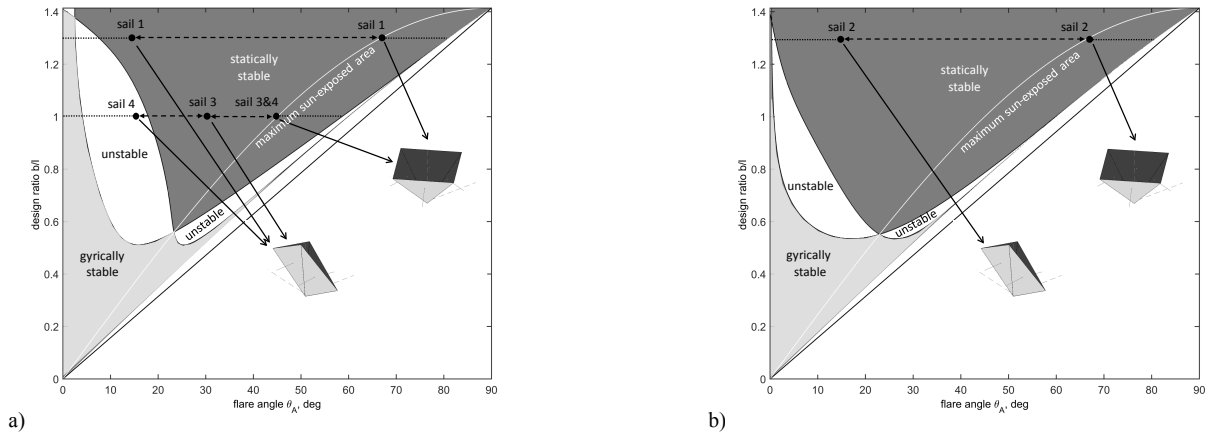


Fig. 4. Heliostable configurations. (a) $l = 1$ m; (b) $l = 2$ m.

Small angular deviations are introduced in order to represent the local vertical direction in the body reference frame as follows:

$$\hat{\mathbf{r}} = [\mathbf{1} - [\boldsymbol{\alpha} \times]] \hat{\mathbf{r}}_0 \quad (17.)$$

where $\hat{\mathbf{r}}_0 = [0 \ 0 \ -1]^T$, as shown in Fig. 3.

The resulting dynamic system is essentially that in Eq. (8.), where the forcing term models the gravity gradient torque. This can be quantified using Eq. (17.), linearizing Eq. (3.), decoupling the pitch-yaw motion and defining the mean motion as $n_0 = \sqrt{\mu/r^3}$, obtaining:

$$\mathbf{T}_{gg} = 3n_0^2 \begin{bmatrix} (I_z - I_y) & 0 \\ 0 & (I_z - I_x) \end{bmatrix} \begin{bmatrix} \alpha_1 \\ \alpha_2 \end{bmatrix} = -\mathbf{K}_{gg} \mathbf{q} \quad (18.)$$

leading to a linearized system which reads as:

$$\mathbf{M}\ddot{\mathbf{q}} + \mathbf{G}\dot{\mathbf{q}} + [\mathbf{K} + \mathbf{K}_{gg}] \mathbf{q} = 0 \quad (19.)$$

Once more the characteristic equation is used, and the set of resulting stable configurations are shaded in Fig. 5 for the two lengths of the sail booms. It can be seen that, in eclipse, for the same length b , the stable region is considerably smaller than in illuminated conditions, as expected due to the lack of restoring SRP torque. However, during the eclipse phase, the flare angle θ_A can be adjusted such to preserve stability.

4. Numerical Simulations

The stability analysis performed in Section 3 neglected that the sun direction slowly changes throughout the year, and the linearized analysis does not take into account this variation. In particular, it is necessary to verify that the heliostability guarantees that the sail $\hat{\mathbf{z}}$ axis (spin axis) can follow the sun direction throughout the year. Furthermore, we must recall that the orbit control strategy described in Section 2.2.4 requires the sail to reconfigure three times per orbit. Such reconfiguration manoeuvres are fast and may compromise the stability of the system even if such stability is guaranteed in a steady state for the three working configurations of the sail. For this reason, a numerical simulation is performed using the model described above to verify the concept and quantify the change in the semi-major axis. As mentioned previously, all numerical results presented in this section consider eclipses, gravity gradient

effects, Earth's oblateness and the Sun's motion along the ecliptic.

The numerical analysis has been performed with four different sails. As set out in Table 2, two different boom lengths are investigated as before ($l=1$ m and $l=2$ m), while the lengths of the base of the sail b have been chosen to satisfy both the stability conditions discussed before and mechanical constraints of the boom hinges¹). The limits on the range of the flare angles of the booms are $15 \text{ deg} \leq \theta_{A,B} \leq 80 \text{ deg}$ and the value of the sail design ratio has been fixed to $b/l=1.3$ for Sail 1 and Sail 2. This design ratio ensures that the sail can perform the requested open/close manoeuvres while maintaining the flare angles inside the admissible ranges and inside the stability regions. The other two configurations (Sail 3 and Sail 4) of the sail are designed with $l=1$ m and $b/l=1$, but different flare angles have been chosen for the mission phases: the fully-closed flare angle of Sails 1, 2 and 3 has been chosen to guarantee their stability, while Sail 4's closed angle has deliberately been chosen to be unstable (see Fig. 4). Finally, the eclipse configurations adopt values so that they might be included in the stable regions of Fig. 5.

The case of the spacecraft initially orbiting in a geostationary orbit is considered, with a control anomaly set to $f_{control} = 60 \text{ deg}$, leading to a fully open configuration of 8 hours, an eclipse mode of 3.7 hours and fully closed configuration of 12.3 hours. The selection of such $f_{control}$ leads to an eclipse starting before and ending after the satellite is in a proper eclipse (which lasts 1.2 hours), in this way it is possible to exploit the heliostabilising effect of the sun-radiation to counteract the transitions between the operative modes.

Table 2. Sails used for the numerical simulations.

		Sail 1	Sail 2	Sail 3	Sail 4*
Boom length, l , m		1	2	1	1
Base of the triangle length, b , m		1.3	2.6	1	1
Flare angle	Fully-closed phase, θ_A^{closed} , deg	15	15	30	15*
	Eclipse phase, $\theta_A^{eclipse}$, deg	55	55	30	30
	Fully-open phase, θ_A^{open} , deg	66.8	66.8	45	45

* Unstable

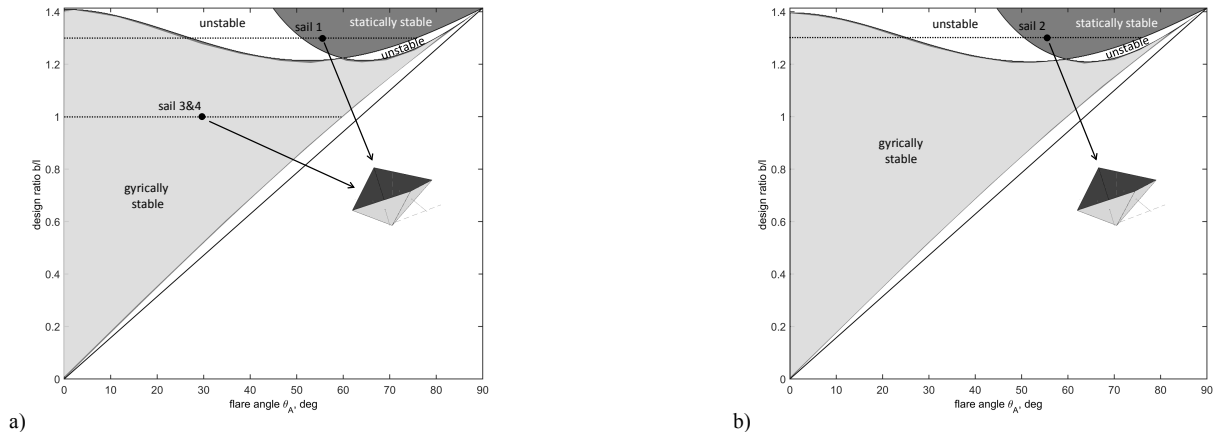


Fig. 5. Stability configurations during the eclipse. (a) $l=1$ m; (b) $l=2$ m.

4.1.Short term behavior

Fig. 6 shows the working mechanism of the variable QRP sail (for the case of Sail 1) during a period of 3 days.

Difficulties in attitude stability occur when the sail enters or exits the eclipse. The yaw and the pitch angles with respect to the sun-pointing direction, as well as the two transversal components of the angular velocity, are plotted in Fig. 7. It is apparent that, during the illuminated phase, the attitude of the spacecraft remains almost aligned to the sun-pointing direction, but during the eclipse the stabilizing effect of the solar radiation is not present and the sail starts drifting from the nominal configuration. As a result, when the solar radiation is recovered, the spin axis of the sail is misaligned with respect to the sun and an impulsive torque is applied that causes severe oscillation of the device. This oscillation can lead to instability, as shown for example in Fig. 7.

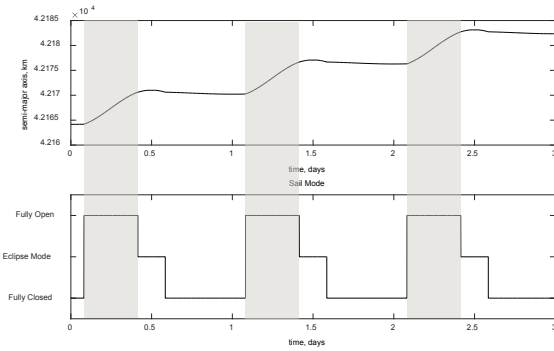


Fig. 6. Orbit raising during the fully opened phases of the sail (Sail 1). Gray bands identify fully-open phases.

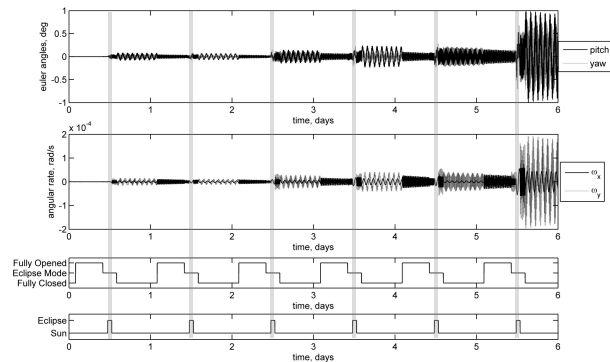


Fig. 7. Attitude with respect to the sun-pointing direction and transversal components of the angular velocity for the undamped case (Sail 1). Gray bands identify eclipses.

4.1.1. Damping

In order to reduce the oscillation amplitude, Ceriotti et al.¹⁾ proposed to equip the spacecraft with passive nutation dampers along \hat{x} and \hat{y} body axes of the sail. These devices usually consist of a sealed ring attached to the spacecraft bus and filled with a viscous fluid. When the spacecraft experiences an angular acceleration, a viscous lag between the bulk fluid and the ring walls dissipates rotational energy as heat¹⁵⁾.

The dampers add an additional viscous torque related to the relative angular velocity of the bulk fluid with respect to the ring¹⁾. The purpose of the dampers is to reduce the oscillation amplitude during the non-eclipse phases such that, at the next

eclipse passage, the sail is almost aligned with respect to the sun.

When the spacecraft reconfigures from the fully-closed to the fully-open configuration a drastic reduction of the transverse components of the angular velocity, as well of the pitch and yaw oscillation amplitude, takes place, see Fig. 8. This change can be explained as the spin rate increases significantly when the sail enters its fully-closed configuration, as highlighted in the gray bands. The increase of the spin rate, due to the changes of moment of inertia, determines a reduction of the transversal components of the angular velocity and therefore reduction of the amplitude of the oscillations perpendicular to the spin direction. Note that it was also numerically verified that the stability/instability of all 4 sails are consistent with the analytical stability study presented in Section 3.

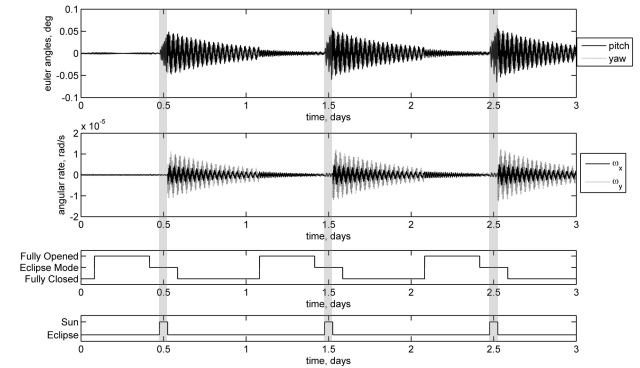


Fig. 8. Pitch and yaw angles with respect to the sun-pointing direction and transversal components of the angular velocity of the Sail 3, with damping. Gray bands identify eclipses.

4.2.Short- and long-term sun pointing

Dissipative fluid rings also play a fundamental role in the long-term sun pointing of the sail. The sun direction slowly changes throughout the year and the attitude of the sail must follow this change. This is achieved by exploiting both the heliostability of the sail and the dissipative effects of the rings. A qualitative explanation of this process can be obtained by focusing on Fig. 9, where a sketch of the sail attitude motion is represented with respect to an inertial reference frame $\hat{c}_1 \hat{c}_2 \hat{c}_3$. Let us assume that initially the \hat{z}_0 axis of the sail, as well as the angular momentum $\hat{\Gamma}_0$, are perfectly aligned along $-\hat{c}_3$, as represented by the dotted, light-gray lines in the figure. If the direction of the sun \hat{r}_s is not perfectly aligned with \hat{c}_3 , as represented in figure, a solar radiation torque is applied to the sail \mathbf{T}_{sr0} . That torque modifies the direction of the angular momentum to $\hat{\Gamma}_1$, leading to an increase of the nutation angle Δ_0 (angle between \hat{z}_0 and $\hat{\Gamma}_1$) and a precession motion of the sail. Therefore the angular momentum of the sail $\hat{\Gamma}$ describes a cone around the direction \hat{r}_s and the body of the sail is moved by the drift angular velocity with respect to $\hat{\Gamma}$ ⁹⁾. In general, the \hat{z} axis of the sail will be misaligned with respect the actual angular momentum $\hat{\Gamma}$ of the sail of a nutation angle Δ and the

dissipative effects of the damping rings becomes mandatory to reduce Δ and to realign the $\hat{\Gamma}$ axis towards the \hat{r}_s direction.

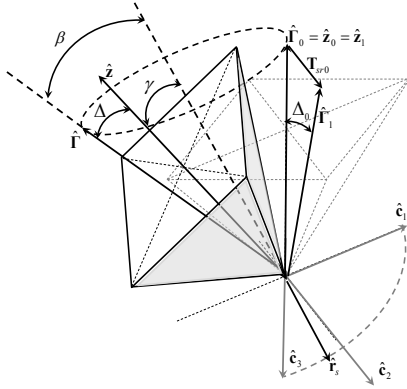


Fig. 9. Long term solar pointing mechanics.

The qualitative behaviour described above is proved by numerical simulations. In Fig. 10 the nutation angle Δ , the angle of aperture of the cone designed by the angular momentum with respect to the sun direction (cone angle β), and the angle between the \hat{z} axis and the sun (pointing angle γ) are plotted for Sail 1. A drift of the \hat{z} axis with respect to the sun pointing direction begins when heliostability is absent (the cone angle and the pointing angles increase), but the main issue is represented by the impulsive behavior of the nutation angle, which increases rapidly when heliostability is recovered. However, the dissipative action of the dampers smoothens it before another eclipse occurs and overall stability is maintained.

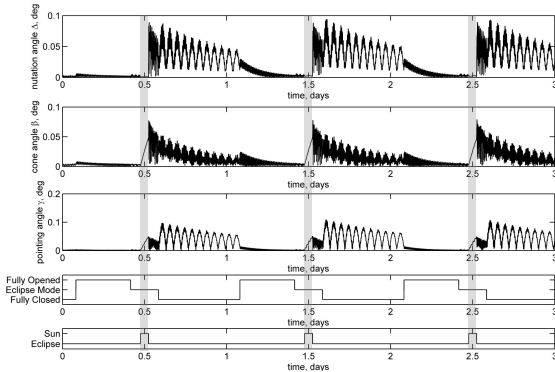


Fig. 10. Nutation, cone and pointing angles (Sail 1).

Year-long simulations are used to show the extended behaviour of the proposed concept. In Fig. 11 the attitudes of Sail 1, Sail 2 and Sail 3 are represented by means the pointing angle γ . It is known that eclipses are present only during specific seasons, and this is reflected in that deviations from the sun-pointing condition increase during these periods compared to other times. It is also noteworthy that the biggest deviation from the nominal working attitude occurs in the case of Sail 2, where some spikes reach an amplitude up to 2.5 deg, while for the other two sails the deviations remain confined in a fraction of degree.

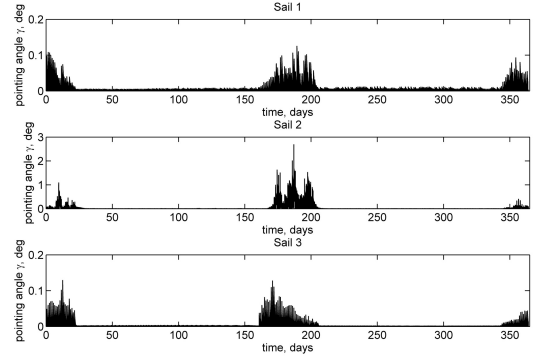


Fig. 11. Pointing angle during one year for Sails 1, 2 and 3.

Finally, the performance in terms of orbit raising of the three configurations have been compared. Table 3 shows the increment of the semi-major axis during one year for the three stable sails, and summarises the core performance indexes. Specifically, Sail 2 obtains the best performance exploiting both its greater area and the high value of the design factor b/l , as also shown in the numeric data summarized in Table 3. A significant increase in altitude is also obtained by Sail 1, but Sail 3, which has a $b/l=1$ and a limited closure angle for stability reasons, cannot perform to a similar degree. The same table shows the averaged decrease of the spin rate over a year for the three sail configurations, and it is therefore suggested that a small heliogyro device may be required to regulate the spin rate over longer missions.

Table 3. Sail performance over 1 year

Performance	Sail 1	Sail 2	Sail 3	Sail 4 *
Orbit raising rate, km/year	$+2.2 \cdot 10^3$	$+8.6 \cdot 10^3$	$+2.8 \cdot 10^2$	-
Maximum sun pointing deviation, deg	$1.3 \cdot 10^{-1}$	$2.7 \cdot 10^0$	$1.3 \cdot 10^{-1}$	$1.8 \cdot 10^2$
Spin decrease rate, rad/(s year)	$-2.8 \cdot 10^{-3}$	$-3.2 \cdot 10^{-3}$	$-6.5 \cdot 10^{-4}$	-
Minimum working orbit altitude, km	$1.7 \cdot 10^4$	$2.8 \cdot 10^4$	$5 \cdot 10^3$	-

* Unstable

Table 3 also summarizes the results of a parametric study performed to find the minimum operable orbit altitude for which the sail may operate despite the increase of the gravity gradient effects on the satellite motion. In fact, in decreasing the altitude of the orbit, both the fraction of orbit in eclipse and the gravity gradient torque magnitude increase, which implies that the analytical results of Fig. 4 and Fig. 5 are no longer valid. Sail 2 provides the worst performance (highest minimum operable altitude) due to its large area and design ratio, while the best performance (lowest minimum operable altitude) is achieved by Sail 3, which exploits its reduced design ratio.

5. Conclusions

The concept of Quasi-Rhombic Pyramid (QRP) solar sail was explored in this paper. The QRP shape provides a passive, self-stabilizing effect around two axes under solar radiation pressure such that the apex of the pyramid passively points towards the Sun, with some support derived from spin about the third axis.

Variation in the boom flare angles changes the effective area-to-mass ratio of the spacecraft and altitude adjustment may be achieved as a consequence.

Analytical, linearized techniques were used to define stability regions of the sail in the configuration space in the short period, and these results were verified for up to one year through numerical simulations. This work took into account full attitude and orbital dynamics, eclipses and gravity gradient torques, in addition to the boom configuration change and revealed that the concept can offer an increase of orbit altitude in the order of few thousand km per year, for a CubeSat-like bus with 1-meter booms in geostationary orbit. Lower increases are to be expected in lower orbits. It is worth underlining that this result is obtained without any expenditure of propellant or need of active attitude control: once the spacecraft is correctly spinning, the only actuation necessary is the opening/closing of the booms. It was also found that the concept becomes unfeasible below approximately 10,000 km a due to the extended duration of the eclipses combined with the magnitude of the gravity gradient torque. It is therefore envisaged that this concept can be used for mid- to high-altitude orbits, such as Geostationary Earth Orbits (GEO): examples are reaching higher orbits, i.e. from Medium Earth Orbit (MEO) to GEO or graveyarding of geostationary spacecraft, particularly when the propellant onboard has been depleted.

References

- 1) Ceriotti, M., Harkness, P. and McRobb, M., "Variable-geometry solar sailing: the possibilities of the quasi-rhombic pyramid", in *Advances in Solar Sailing*, Macdonald, M., Editor. 2014, Springer Berlin Heidelberg, p. 899-919. ISBN: 978-3-642-34906-5. DOI: 10.1007/978-3-642-34907-2_54
- 2) Macdonald, M. and McInnes, C. R., "Analytical control laws for planet-centred solar sailing", *Journal of Guidance, Control, and Dynamics*, vol. 28, n. 5, p. 1038-1048, 2005. DOI: 10.2514/1.11400
- 3) Wie, B. and Murphy, D., "Solar-Sail Attitude Control Design for a Flight Validation Mission", *Journal of Spacecraft and Rockets*, vol. 44, n. 4, p. 809-821, 2007. DOI: 10.2514/1.22996
- 4) Funase, R., Shirasawa, Y., Mimasu, Y., Mori, O., Tsuda, Y., et al., "On-orbit verification of fuel-free attitude control system for spinning solar sail utilizing solar radiation pressure", *Advances in Space Research (Special issue Solar Sailing)*, vol. 48, n. 11, p. 1740-1746, 2011. DOI: 10.1016/j.asr.2011.02.022
- 5) Wie, B., "Solar sail attitude control and dynamics, part 1", *Journal of Guidance, Control, and Dynamics*, vol. 27, n. 4, p. 526-535, 2004. DOI: 10.2514/1.11134
- 6) Tsuda, Y., Mori, O., Funase, R., Sawada, H., Yamamoto, T., et al., "Flight status of IKAROS deep space solar sail demonstrator", *Acta Astronautica*, vol. 69, p. 833-840, 2011. DOI: 10.1016/j.actaastro.2011.06.005
- 7) Ceriotti, M., Harkness, P. and McRobb, M., "Variable-geometry solar sailing: the possibilities of the quasi-rhombic pyramid", in *Proceedings of 3rd International Symposium on Solar Sailing (ISSS 2013)*, Glasgow, UK, 2013.
- 8) Molostov, A. A. and Shvartsburg, A. A., "Heliocentric halos for a solar sail with absorption", *Soviet Physics Doklady*, vol. 37, n. 4, p. 149-152, 1992.
- 9) Hughes, P. C., "Spacecraft attitude dynamics", Dover Publications, Inc., Mineola, NY, USA, 2004.
- 10) McInnes, C. R., "Artificial Lagrange points for a partially reflecting flat solar sail", *Journal of Guidance, Control, and Dynamics*, vol. 22, n. 1, p. 185-187, 1999. DOI: 10.2514/2.7627
- 11) Krivov, A. V., Sokolov, L. L. and Dikarev, V. V., "Dynamics of Mars-orbiting dust: Effects of light pressure and planetary oblateness", *Celestial Mechanics and Dynamical Astronomy*, vol. 63, n. 3-4, p. 313-339, 1995. DOI: 10.1007/bf00692293
- 12) Schaub, H. and Junkins, J. L., "Analytical Mechanics of Space Systems, 2nd Edition", *AIAA Education Series*, ed. Schetz, J.A., Reston, VA, USA 2009.
- 13) Battin, R. H., "An introduction to the mathematics and methods of astrodynamics", Revised edition, *AIAA Education Series*, AIAA, New York, 1999. ISBN: 1-56347-342-9
- 14) Harkness, P. G., McRobb, M., Lützkendorf, P., Milligan, R., Feeney, A., et al., "Development status of AEOLDOS – A deorbit module for small satellites", *Advances in Space Research*, vol. 54, n. 1, p. 82-91, 2014. DOI: 10.1016/j.asr.2014.03.022
- 15) Nobari, N. A. and Misra, A. K., "Attitude Dynamics and Control of Satellites With Fluid Ring Actuators", *Journal of Guidance, Control, and Dynamics*, vol. 35, n. 6, p. 1855-1864, 2012. DOI: 10.2514/1.54599